Aerosol hygroscopic properties as measured by lidar and comparison with in situ measurements

Graham Feingold
Environmental Technology Laboratory, NOAA, Boulder, Colorado, USA

Bruce Morley
Atmospheric Technology Division, National Center for Atmospheric Research, Boulder, Colorado, USA

Received 13 August 2002; revised 24 October 2002; accepted 26 February 2003; published 3 June 2003.

[1] We demonstrate the ability of a single-wavelength backscatter lidar to provide information on the uptake of water vapor by aerosol in a well-mixed, cloud-capped, boundary layer. Aerosol hydration has important consequences for the effect of aerosols on the Earth's radiation budget. A vertically pointing, airborne lidar is used to measure vertical profiles of aerosol backscatter beneath a stratocumulus cloud deck. In situ aircraft thermodynamic measurements are used to derive simultaneous profiles of relative humidity (RH) under the assumption that the boundary layer is well mixed. The change in backscatter is derived as a function of relative humidity over the range ~85% RH to ~98.5% RH. In situ measurements of the aerosol size distribution and composition are used to calculate the expected enhancement in backscatter due to equilibrium uptake of water vapor. Comparison between lidar backscatter enhancement as a function of RH and that derived from the in situ aerosol size distribution and composition measurements shows good agreement. Conditional sampling on strong updrafts/downdrafts indicates that aerosol backscatter tends to be higher in downdrafts than it is in updrafts for the same RH range. This is consistent with the concept of inertia of the larger hydrated particles to growth/evaporation at short timescales but may also be due to a bias in the way that lidar-derived cloud base is interpreted in updrafts versus downdrafts. Calculations of enhancement in total scatter due to water vapor uptake with enhancement in backscatter suggest that the effects agree to within ~20% of one another for RH < ~95% but that they differ significantly for RH > 95%. *INDEX TERMS:* 0305 Atmospheric Composition and Structure: Aerosols and particles (0345, 4801); 0320 Atmospheric Composition and Structure: Cloud physics and chemistry; 0360 Atmospheric Composition and Structure: Transmission and scattering of radiation; 3360 Meteorology and Atmospheric Dynamics: Remote sensing; 1640 Global Change: Remote sensing; *KEYWORDS:* aerosol water vapor uptake, backscatter, lidar

Citation: Feingold, G., and B. Morley, Aerosol hygroscopic properties as measured by lidar and comparison with in situ measurements, *J. Geophys. Res.*, *108*(D11), 4327, doi:10.1029/2002JD002842, 2003.

1. Introduction

[2] Atmospheric aerosol particles have received much attention in recent decades because of their importance in climate change. The extent to which these particles modify the Earth's radiative budget depends on a number of factors, including their size distribution and composition. Global mapping of aerosol is a particularly challenging problem given the extreme variability in aerosols, be they of natural or anthropogenic origin.

[3] This work addresses a particular aspect of aerosol, namely, the extent to which they have an affinity for water vapor. The size increase of aerosol particles resulting from uptake of water vapor has important implications for the direct scattering of radiation (the "direct effect") [e.g., *Hegg et al.*, 1996]. It also has bearing on the ability of these particles to serve as cloud condensation nuclei (CCN) and, under the right circumstances, to form cloud droplets (the "indirect effect"). *Twomey* [1974] noted that an increase in aerosol concentrations due to anthropogenic sources would result in an increase in CCN and therefore an increase in droplet number concentration. This would result in clouds that reflect more shortwave radiation to space, all other conditions (primarily liquid water path) being equal. However, as noted by *Eichel et al.* [1996] and *Wulfmeyer and Feingold* [2000], this chain of events may not be a foregone conclusion. For example, if anthropogenic aerosols are less hygroscopic, they will be less effective as CCN, and increases in aerosol concentrations may not simply translate to increases in CCN and cloud droplet concentrations. The possibility of feedback mechanisms whereby increases in the abundance of aerosols, or changes in their composition, may reduce cloudiness [*Han-*

Copyright 2003 by the American Geophysical Union.
0148-0227/03/2002JD002842$09.00

sen et al., 1997; *Brenguier et al.*, 2000; *Jiang et al.*, 2002] must also be taken into account.

[4] In a recent paper, *Wulfmeyer and Feingold* [2000] (henceforth WF) showed how a differential absorption lidar (DIAL) can be used to infer the extent of water vapor uptake by aerosols. A vertically pointing DIAL simultaneously measures the water vapor concentration and aerosol backscatter in the same sample volume. If the boundary layer is well mixed, i.e., the aerosol size distribution is constant with height, then any change in backscatter in the vertical is due to uptake of water vapor by the particles. Using clouds as calibration points (cloud base is saturated), and assuming that the potential temperature is constant with height, the relative humidity RH profile can be calculated. WF presented backscatter growth factors for data taken at Gotland in the Baltic Sea. After a rigorous analysis of the technique it was shown that the rather modest increases in backscatter with RH were suggestive of an aerosol with low mass fraction ($\sim$25%) of soluble material. However, there were no in situ aerosol measurements to confirm this. Raman lidar, which also has the ability to simultaneously measure backscatter (or extinction) and water vapor concentration, has also been applied to measurement of hygroscopic growth [e.g., *Ferrare et al.*, 1998].

[5] The lidar method for determining hygroscopic growth has numerous advantages, including the fact that (1) enhancement in backscatter due to changes in RH is measured under ambient, unperturbed atmospheric conditions and (2) the range of measurement can be extended to very close to saturation. The traditional method of measuring this growth factor uses a scattering nephelometer that aspirates an air sample, dries it, and then reexposes it to varying levels of RH, typically 65%, 75%, and 85% [*Charlson et al.*, 1984; *Hegg et al.*, 1996; *McInnes et al.*, 1998]. The growth in total scattering is referred to as f(RH) [*Charlson et al.*, 1992]. Humidified nephelometers cannot expose air samples to RH > $\simeq$85% without risking condensation on their chilled mirrors and spurious measurements. Humidified tandem differential mobility analysers (HTDMAs) have the advantage of being able to size-select aerosol particles before exposing them to controlled humidity environments so that aerosol hygroscopicity can be determined as a function of size. HTDMAs also have difficulty achieving high RH although measurements at RH $\simeq$ 90% are possible [e.g., *Brechtel and Kreidenweis*, 2000], and yet the region of 85% < RH < 100% is of great interest because it is here that particles experience their most dramatic growth. Moreover, the extent of this growth hints at their ability to act as CCN.

[6] A number of questions remain unanswered which this paper will address: (1) Can a lidar-equivalent f(RH) be derived from the more common backscatter lidars? There exist only a few DIAL instruments capable of performing this measurement, which would limit its usefulness. (2) What is the relationship between the nephelometer-derived f(RH) (i.e., based on total scatter) and that derived from a backscatter lidar f_β(RH)? (3) Is there consistency between the lidar-derived f_β(RH) and in situ measurements of aerosol size distribution and composition? (4) Can one demonstrate successful use of this method for long time series of data? (WF analyzed only 1-min worth of data.)

[7] We begin with a description of the field experiment (Dynamics and Chemistry of Marine Stratocumulus-II or DYCOMS-II) that enabled this measurement; we then follow with a brief outline of the technique, present the results, and discuss their implications.

2. Experiment

[8] The DYCOMS-II field experiment [*Stevens et al.*, 2003] took place during the month of July 2001 and addressed scientific issues related to the stratocumulus cloud regime off the coast of southern California. Flights focused on the region around 31°N, 122°W, over the open ocean and approximately 400 km from the mainland. The primary goal of the experiment was to quantify entrainment rates at the boundary layer inversion under nocturnal conditions. Other, related experiments addressed the effect of aerosols on cloud microphysics and drizzle formation in stratocumulus. The National Center for Atmospheric Research (NCAR) fielded its fully instrumented C-130 aircraft which measured thermodynamic variables, aerosol size distributions, cloud microphysics, atmospheric trace gases, and radiation. The two-wavelength Scanning Aerosol Backscatter Lidar (SABL) is the primary source of data for this study. The Nd-Yag laser operates at the fundamental and doubled frequencies corresponding to wavelengths of 1.064 μm and 0.532 μm; it has a pulse length of 15 ns and a pulse rate of 20 Hz. The range resolution is 3.75 m. Only the 0.532 μm channel is used in this study because of detector saturation/recovery problems at 1.064 μm. Most of SABL is in an instrumentation pod under the left wing outboard of the engines. This includes the transmitter/receiver module and associated electronics. The SABL control interface, display, and data recording functions are in the main cabin. The mission scientist on the flight deck can also view a display of the range-corrected data in real time. SABL operated in a vertically pointing mode and was used primarily for detecting the fine structure of cloud top height. However, during most flights a level flight leg was flown just above the sea surface with the lidar looking vertically up at cloud base. These low-level legs were typically of 30- to 60-min duration and took place at about 1300 UTC (0500 local time).

[9] The nocturnal stratocumulus-capped boundary layer was characterized by very well mixed conditions, as documented by regular aircraft profiles. Clouds were typically a few hundred meters thick, and the skies were overcast. Drizzle was quite pervasive, but since drizzle drops contaminate the aerosol return, drizzling periods are avoided in the current study.

3. Description of the Technique

[10] As done by WF, a vertically pointing lidar is used to calculate simultaneous profiles of aerosol backscatter β and RH in the same volume of air. The method is applied only in well-mixed boundary layers, where it can be assumed that any changes in β are due to changes in RH rather than a change in the equivalent dry aerosol size distribution. WF used DIAL to measure a profile of water vapor concentration, and thermodynamic arguments for a well-mixed boundary layer were invoked to calculate an RH profile. This essentially required inferring the virtual potential temperature θ_v at cloud base from the assumption that cloud

base is saturated and assuming that θ_v is constant with height.

[11] Here the method is extended for use with a single-wavelength backscatter lidar. As with the DIAL measurement a backscatter profile is measured by the lidar. However, in the absence of an independent water vapor measurement, the assumption is made that both the potential temperature θ and water vapor mixing ratio r_v are constant with height, a valid assumption for well-mixed boundary layers. These assumptions enable use of a number of approaches for calculation of the RH profile. Examples are as follows:

[12] 1. The in situ measurements of r_v and θ are used and assumed invariant with height. Cloud base is determined as the point when water vapor saturation is reached. One can check the accuracy of this method by calculating the thermodynamically derived cloud base and comparing it with that observed by the lidar. Cloud base is characterized by a very sharp increase in β, and accuracy in its measurement is on the order of ±10 m (see WF).

[13] 2. Because lidar can detect cloud base to high accuracy, the lidar-derived cloud base can be assumed to be the true cloud base. First, a temperature profile is derived from the θ measurement and the assumption of a hydrostatic atmosphere. The cloud base temperature T_{cb} and cloud base pressure P_{cb} are calculated. Then, under the assumption of 100% RH at cloud base the cloud base water vapor pressure e_{cb} can be calculated as

$$e_{cb} = e_s(T_{cb}), \tag{1}$$

where e_s is the saturated water vapor pressure and is only a function of temperature T. The cloud base mixing ratio r_v can then be calculated as

$$r_v = \frac{0.622 e_{cb}}{P_{cb} - e_{cb}}, \tag{2}$$

where P_{cb} is the cloud base pressure. Finally, the RH profile is calculated using

$$e(z) = \frac{r_v P(z)}{0.622 + r_v} \tag{3}$$

and

$$\mathrm{RH}(z) = \frac{e(z)}{e_s[T(z)]}. \tag{4}$$

[14] The lidar derives cloud base using a gradient algorithm that looks for a very large increase in lidar return signal amplitude. During DYCOMS-II the receiver was saturated by the signal from the cloud, and cloud base was determined as the range at which the signal was halfway to saturating the receiver (digitizer). Comparison of cloud base derived by lidar with that based on method 1 shows strong, time-dependent biases that have been traced to inaccuracies in the Lyman-α hygrometer (Figure 1). For this reason we opt to use method 2 in our analysis.

4. Results

4.1. Lidar Observations

[15] We focus on research flight 1 on 10 July 2001. The boundary layer met the primary criteria of being well-mixed and having no detectable subcloud drizzle. From approximately 12.5 to 13.5 UTC (fractional hours) the aircraft flew a low-level leg beneath the cloud (Figure 2). Cloud base, as shown by the lower edge of the "orange layer" is at about 450–500 m. The cloud base height detection routine is used to record cloud base at a frequency of 1 Hz (Figure 1). Backscatter profiles are analyzed at the same frequency, as are profiles of RH, following the procedure outlined in section 3 (equations (1)–(4)). The lidar measures returned power as

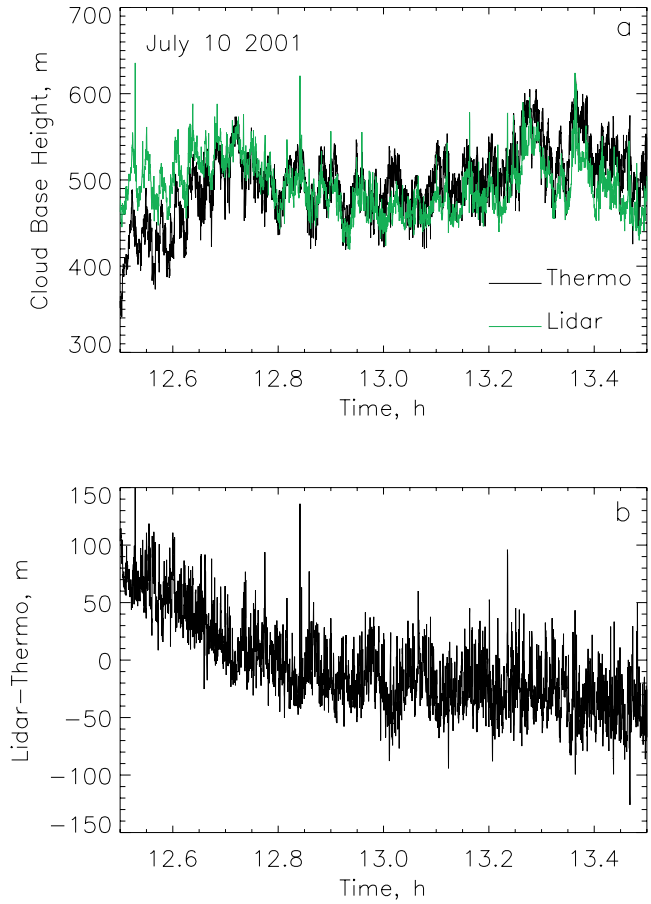

Figure 1. (a) Cloud base height derived assuming a well-mixed boundary layer as described in method 1 in the text ("Thermo"), compared with the lidar-measured cloud base height ("Lidar"). In deriving the Thermo cloud base height, a correction of 0.275 g kg^{-1} was applied (subtracted) as suggested by B. Stevens (personal communication, 2002). Note that prior to the time period shown, the aircraft was flying in cloud, and the Lyman-α probe probably suffered from wetting. (b) Lidar-derived cloud base minus Thermo-derived cloud base as a function of time (UTC, fractional hours) showing significant time-dependent differences.

$$P(R,\lambda) = \frac{C}{R^2}\beta(\lambda,R)e^{-2\int_0^R \alpha(\lambda,R)dR}; \tag{5}$$

β is the lidar backscatter, α is the lidar extinction, C is a system constant, R is the range to the target volume, and λ is the wavelength (= 0.532 μm). Lidar returned-power profiles are range-corrected to yield uncalibrated attenuated backscatter profiles. As such they are ambiguous since a single

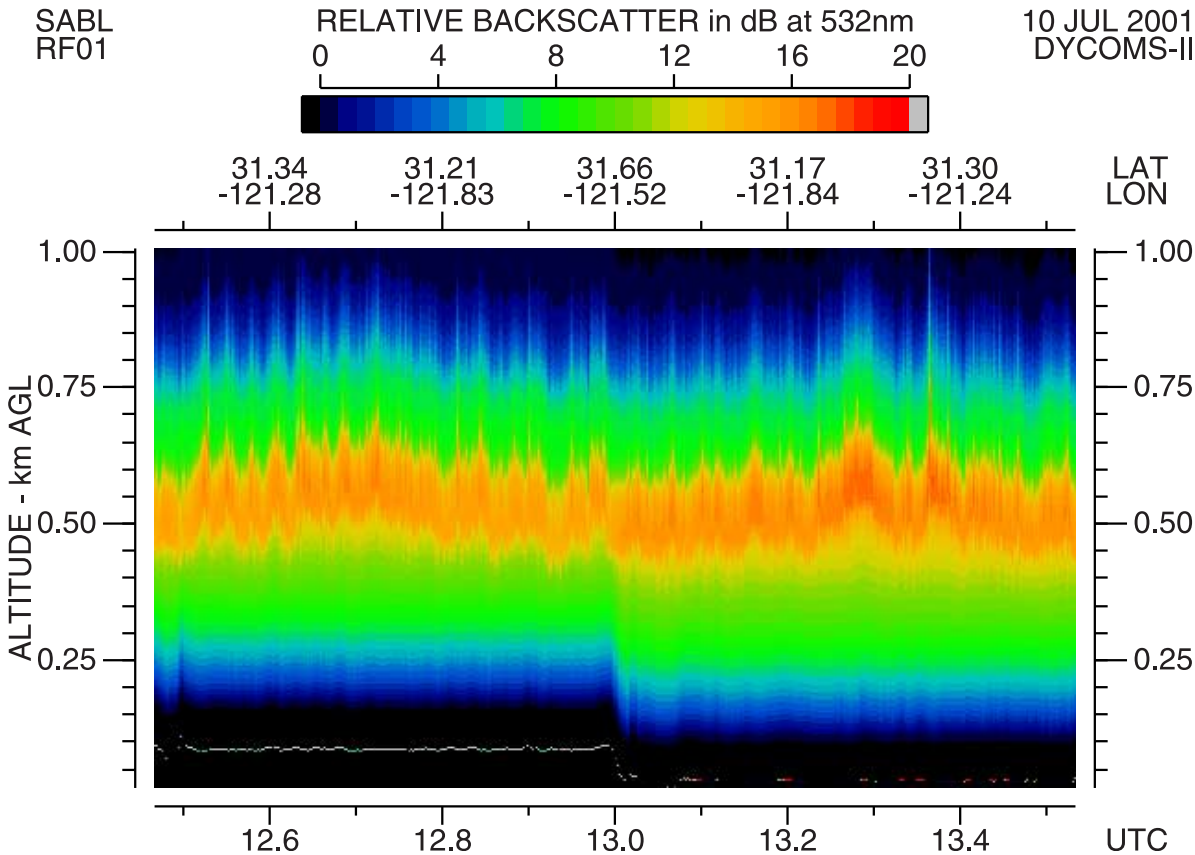

Figure 2. Lidar profiles of range-corrected backscatter in units of dB for the period of interest. Cloud base, as shown by the lower edge of the "orange layer" is at about 450–500 m. At approximately 13.0 UTC the aircraft lowered its altitude.

measurement depends on two unknowns, β and α. The normal procedure to remove this ambiguity is to use an assumed ratio of α to β:

$$S = \frac{\alpha}{\beta}. \tag{6}$$

As shown by WF, the derivation of backscatter-derived f_β(RH) is very weakly ependent on the assumed value of S. This will be discussed in section 5.1.

[16] Lidar backscatter data are corrected for attenuation using a simple forward technique, assuming that at the first range gate β is equal to the attenuated backscatter. A value of $S = 90$ sr is assumed. In addition, a calibration factor of 10^{-7} m^{-1} sr^{-1} is assumed since the lidar records relative power rather than calibrated backscatter. In order to calculate f_β(RH), β at range R is normalized to β at RH $\simeq$ 85%, corresponding to the height of the first useful lidar data (full overlap). Calculations indicate that the contributions of molecular backscatter and extinction to total backscatter and extinction have a small effect on this normalized measurement (<4%); these corrections have not been applied to the data.

[17] Figure 3 shows a plot of β (RH) normalized by β (RH = 85%) as a function of RH for 30 min of data (13.0–13.5 UTC). Each profile represents a 1-s sample. A bold solid line represents the mean value in selected RH bins, and horizontal bars indicate the tenth and ninetieth percentiles in each of these bins. A rather steep increase in f_β(RH)

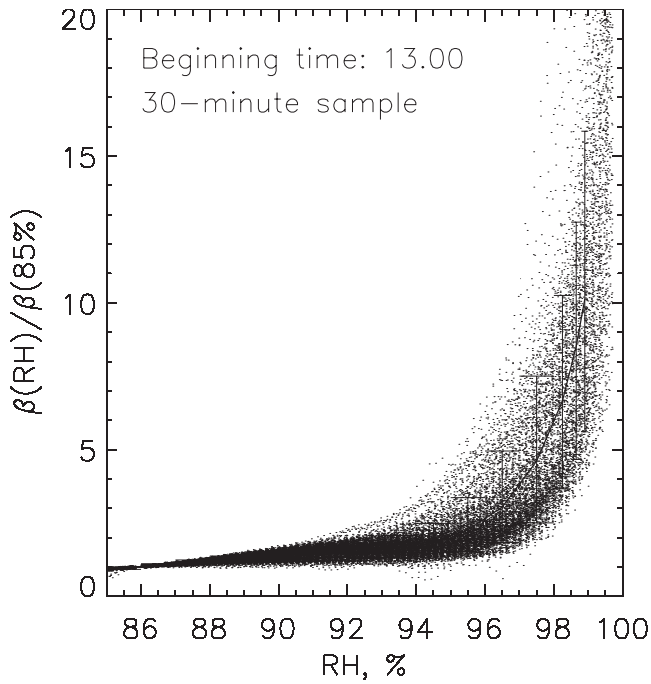

Figure 3. Enhancement in lidar backscatter β normalized by β at 85% RH as a function of RH. Individual profiles (data points) represent 1-s samples. The mean, tenth, and ninetieth percentiles are plotted in selected RH bins.

is observed with mean values reaching 10 at 98.9%. These values are much larger than those obtained by WF in a polluted Baltic Sea location. There, the equivalent value of $\beta(98\%)/\beta(85\%)$ was ≈ 2.1.

[18] The variability in f_β(RH) is a function of a number of factors, including the aerosol size distribution and/or composition as well as deviations in the boundary layer from a well-mixed state and therefore inaccuracies in the derived RH profile. These are particularly pronounced at high RH. Note that because f_β(RH) is a ratio, its accuracy would not be dependent on lidar calibration if f_β(RH) were expressed in terms of attenuated backscatter, but because f_β(RH) is expressed in terms of unattenuated backscatter, it is weakly dependent on the assumed calibration. It is also weakly dependent on the assumed value of S. These sensitivities are explored in section 5.1.

4.2. Comparison With Calculations Based on In Situ Aerosol Measurements

[19] The NCAR C-130 was equipped with a Passive Cavity Aerosol Spectrometer (PCASP) that measures aerosol particles in the size range 0.1–3 μm (diameter). Heating elements were applied to the instrument, which had the salutary effect of drying the particles. This particular instrument sorted the particles into 30 individual size bins, the specifications for which assume that particles are spherical and have a refractive index of 1.58. In situ analyses duing DYCOMS-II (J. Anderson et al., manuscript in preparation, 2003) suggest that the aerosol was predominantly sodium chloride (NaCl). The real part of the refractive index of NaCl (dry) is 1.55 at 0.532 μm so that undersizing due to refractive index differences is minor [*Hand et al.*, 2000] if the particles are indeed dry. Figure 4 shows a time series of number concentration N_a, mean radius $\bar{r}$, and relative dispersion D (equal to standard deviation normalized by $\bar{r}$) for the time period 13.0–13.5 UTC. Average values of N_a, $\bar{r}$, and D are 175 3, 0.08 μm, and 0.52, respectively. (Equivalent lognormal parameters are median radius r_g = 0.07 μm and geometric standard deviation σ = 1.63.) We note that there is no apparent change in the size spectrum prior to and after 13.0 UTC when the aircraft changed altitude (Figure 2). The aerosol fields experience a perturbation during descent, but once the aircraft returns to a level position, aerosol size distribution parameters are restored. This provides confidence that aerosol spectra were measured in their dry state. At about 13.35, there is a marked shift in the size spectra (Figure 4) as characterized by sharp increases in N_a and $\bar{r}$ and a decrease in D.

[20] Comparison of the lidar-derived f_β(RH) with PCASP data entails calculation of β based on the aerosol size distribution $n(r)$:

$$\beta = \int_{r_{min}}^{r_{max}} Q_\pi(r, m)\pi r^2 n(r) dr, \tag{7}$$

where $Q_\pi(r, m)$ is the backscatter efficiency at radius r and refractive index m and r_{min} and r_{max} correspond to the lower and upper bounds of the PCASP, respectively. (Again the wavelength dependence is implicit.) Figure 5 shows β based on the PCASP size spectra (at 1-s temporal resolution) over the same time period as Figure 3. The aerosol composition is assumed to be pure NaCl. Particles are assumed to be at equilibrium with their environment, and their growth is calculated according to *Pruppacher and Klett* [1997, p. 176]. The refractive index is calculated using the volume mixing law and is therefore RH-dependent. Individual profiles are calculated at the RH values corresponding to a fixed height grid with Δz = 3.75 m. For clarity, only the mean, tenth percentile, and ninetieth percentile values are shown. Figure 5 also superimposes the mean f_β(RH) from the lidar data in Figure 3. It can be seen that the mean lidar profile falls close to the mean PCASP profile over most of the RH range. Above RH = 96% the lidar tends to overestimate f_β(RH), but, in general, the agreement is reasonable.

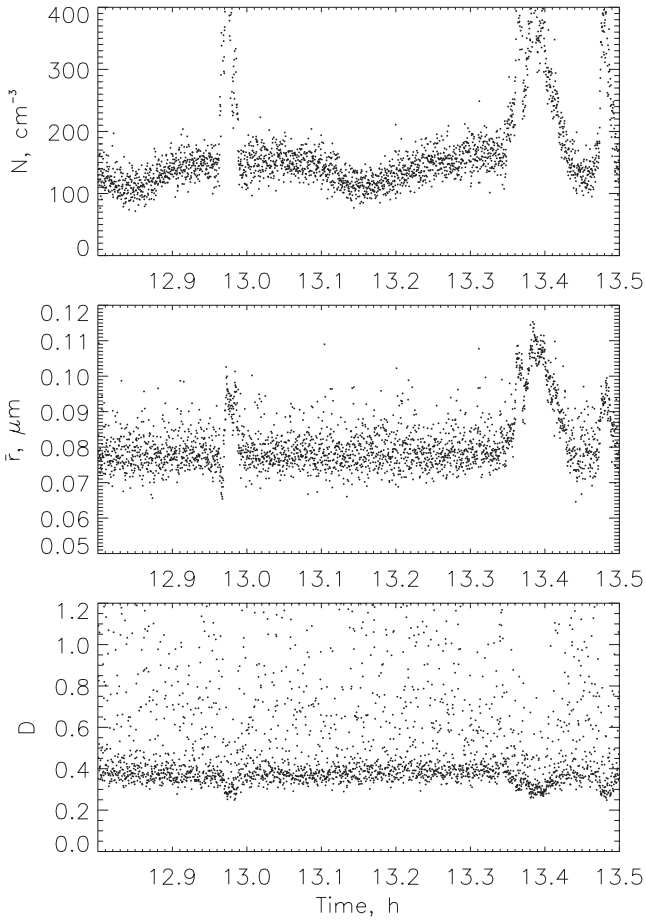

Figure 4. Time series of aerosol size distribution parameters measured by the Passive Cavity Aerosol Spectrometer (PCASP) over the period of interest. Between 13.0 and 13.3 UTC the size distributions are approximately constant. Thereafter, there is a marked increase in N_a and $\bar{r}$ and a decrease in D.

5. Discussion

5.1. Sensitivity to Assumed Values of Calibration and *S*

[21] Results in Figure 3 are recalculated using different assumptions for the assumed $S = \alpha/\beta$ and assumed calibration constant. S is changed from 90 sr to 50 sr, and the calibration constant is changed from 10^{-9} m^{-1} sr^{-1} to 10^{-6} m^{-1} sr^{-1} (recall that Figure 3 used S = 90 sr and a calibration constant of 10^{-7} m^{-1} sr^{-1}). Figure 6 shows the mean profiles for combinations of S and calibration

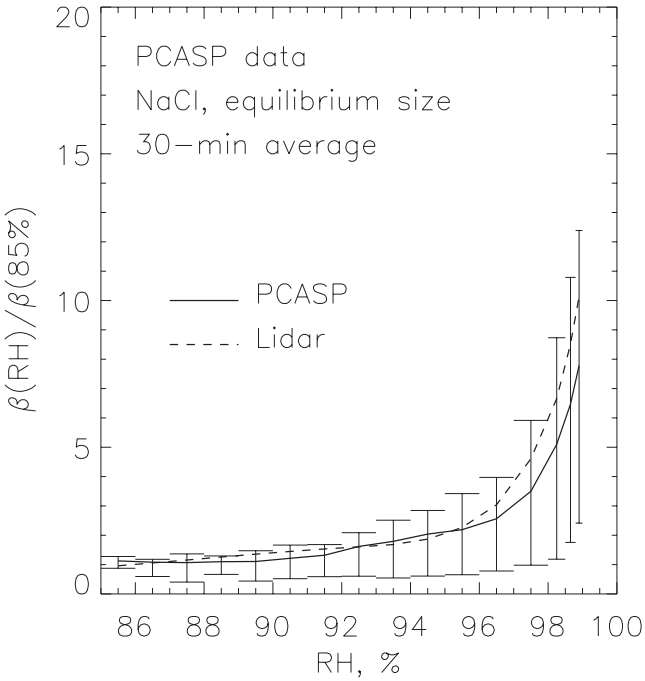

Figure 5. As in Figure 3, but with β(RH) calculated based on in situ PCASP size spectra and the assumption that particles are fully soluble NaCl. Uncertainty bars represent the tenth and ninetieth percentiles for the PCASP data. The mean values from Figure 3 are superimposed for comparison.

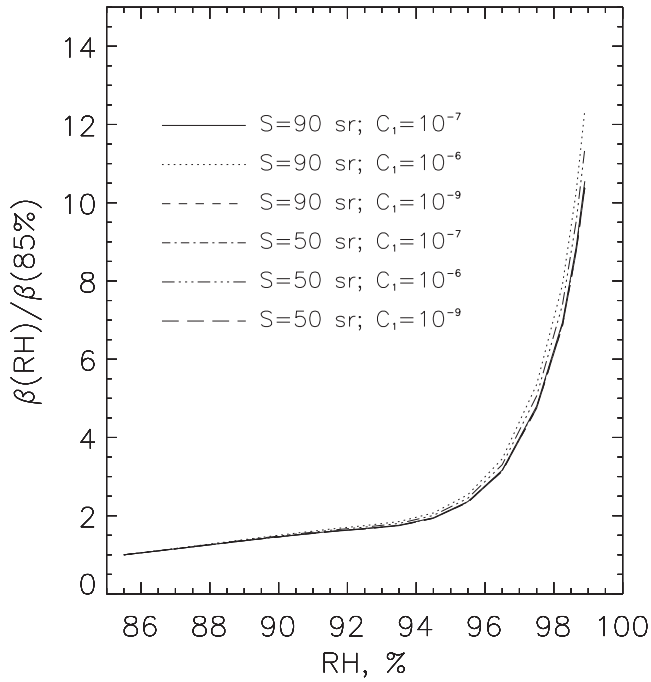

Figure 6. As in Figure 3, but showing sensitivity of the mean f_β(RH) to the assumed value of S and assumed calibration constant. S is either 50 or 90 sr, and the calibration constant is varied over 3 orders of magnitude from 10^{-9} m^{-1} sr^{-1} to 10^{-6} m^{-1} sr^{-1}.

constant. It can be seen that there is very weak sensitivity to the assumed values. The largest difference from the base result in Figure 3 is for S = 90 sr and a calibration constant of 10^{-6} m^{-1} sr^{-1} (dotted line), particularly at the highest RH. However, the differences are far smaller than the variability between individual profiles over the 30-min analysis period (Figure 3).

[22] We note that numerous studies have investigated the effect of RH on S. Modeling studies [e.g., *de Leeuw et al.*, 1986] and our calculations show that S is approximately constant with RH over the range 80% < RH < 97%. The backscatter nephelometer measurements of *Anderson et al.* [2000] show a great deal of variability in S, very little of which can be explained by RH. We applied our model to the region of RH > 97% and found that the behavior of S is dependent on the aerosol size distribution and composition. Our lidar-derived f_β(RH) assumes a constant S, but according to Figure 6, even if large changes in S do occur for RH > 97%, changes to f_β(RH) would be relatively small and would not alter the main results in Figures 3 and 5.

5.2. Sensitivity to Cloud Base Measurement

[23] The method used here relies on a lidar measure of cloud base height to derive the RH profile. Lidars observe cloud base as a very hard target, and error in this measurement should be small. The sensitivity of f_β(RH) to an assumed error of ±10 m in cloud base height is calculated and shown in Figure 7. For RH < 95%, there is no difference in the mean values of f_β(RH) for the three cases considered. As RH increases above 95%, there is a progressive increase in the error in f_β(RH). For example, at RH = 96.5% the difference is ±∼12%, and at 98.9% the difference is ±∼50%. The increased sensitivity to cloud base height with increasing RH is expected; it results from the nonlinearity of the dependence of saturation vapor pressure on temperature, because small changes in cloud base height (and therefore temperature) translate to larger

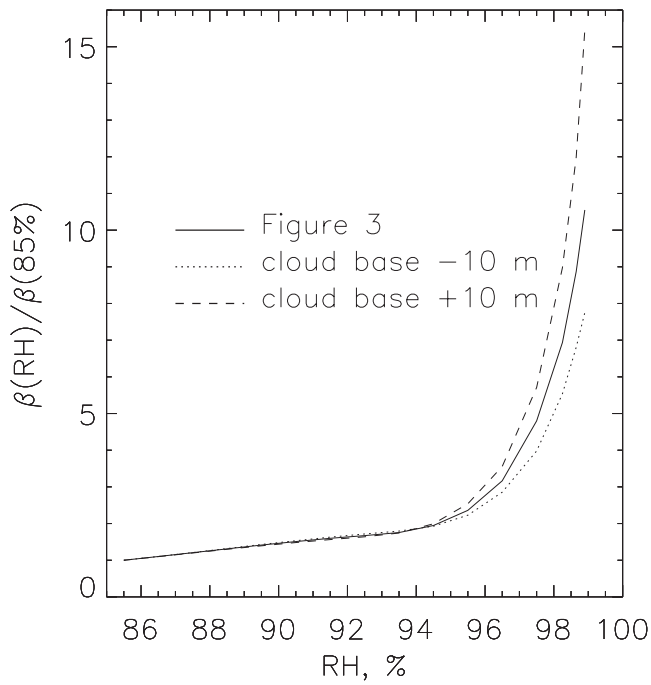

Figure 7. As in Figure 3, but showing sensitivity of the mean f_β(RH) to the measurement of cloud base height.

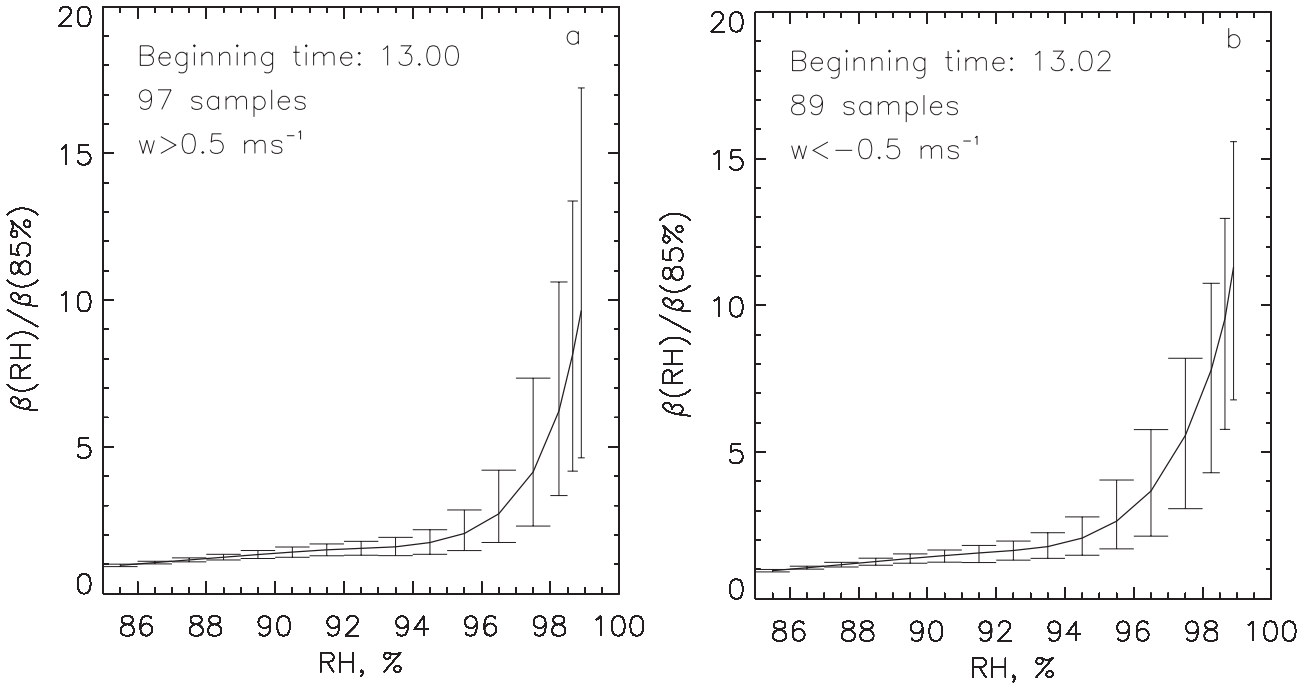

Figure 8. As in Figure 3, but for conditional sampling on updraft velocity w: (a) $w > 0.5$ m s^{-1} and (b) $w < -0.5$ m s^{-1}.

changes in saturation vapor pressure. The issue of how inaccuracies in the way lidar observes cloud base, which is based on backscatter, as opposed to a saturation point, is explored further in section 5.3.

5.3. Conditional Sampling for Updrafts/Downdrafts

[24] The NCAR C-130 is equipped with a gust probe that records vertical velocity w during the course of a flight. The question arises whether there are any systematic differences between f_β(RH) in updrafts and downdrafts. Figure 8 shows plots of f_β(RH) for the stronger updrafts/downdrafts, with a threshold of ±0.5 m s^{-1}. It is noted (Figure 9a) that the downdrafts tend to have higher f_β(RH) than the updrafts for all values of RH. The data were analyzed over shorter time periods and with somewhat different thresholds (Figure 9b), and in all cases this feature is qualitatively robust. The

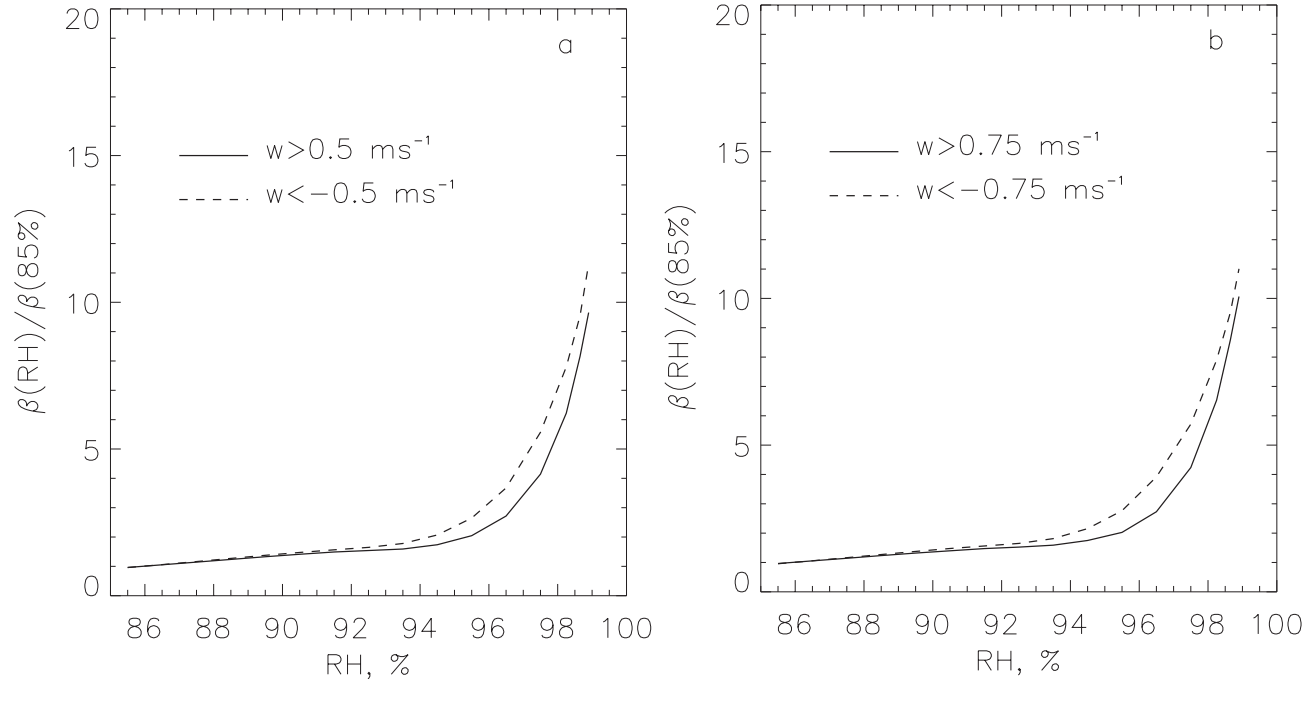

Figure 9. As in Figure 3, showing only the mean values of increases in backscatter with RH: (a) $w > 0.5$ m s^{-1} and $w < -0.5$ m s^{-1} and (b) $w > 0.75$ m s^{-1} and $w < -0.75$ m s^{-1}.

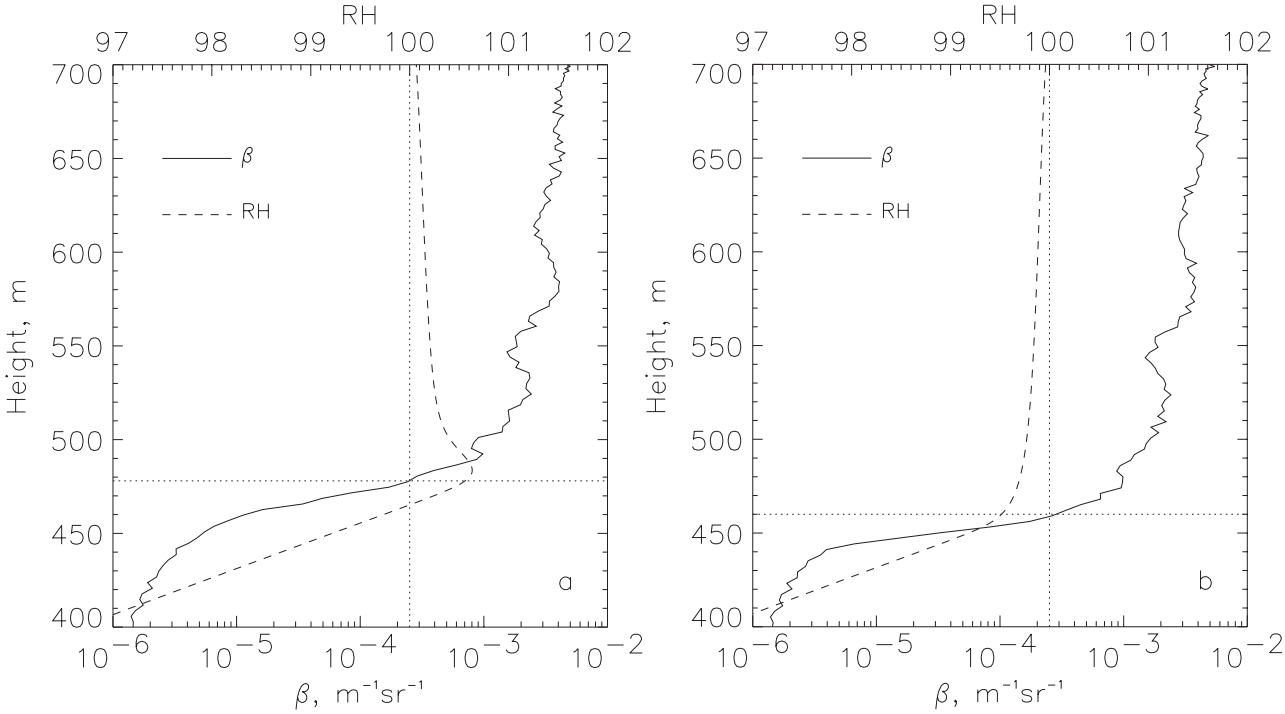

Figure 10. β and RH as a function of height as simulated by an adiabatic parcel model for an updraft/downdraft sequence: (a) $w > 0$ and (b) $w < 0$.

differences in f_β(RH) tend to increase with increasing w. For example, at 96.5% RH the difference in f_β(RH) is 35% for $w = \pm 0.5$ m s^{-1} and 44% for $w = \pm 0.75$ m s^{-1}. We have identified two sources that explain the tendency for downdrafts to exhibit higher growth factors than updrafts do at the same RH:

[25] The first source is inertia to growth/evaporation. In the stronger updrafts, larger particles do not have time to achieve equilibrium size. According to *Feingold et al.* [1994], at an updraft of 0.5 m s^{-1}, only particles <0.05 μm radius (dry) will achieve their equilibrium sizes. Thus the majority of particles to which the 0.532 μm lidar is sensitive will have subequilibrium sizes in an updraft of 0.5 m s^{-1}; this will translate to lower f_β(RH). Conversely, downdrafts emerging from cloud base tend to contain evaporating drops that have finite time constants associated with evaporation, and this inertia to evaporation translates to higher f_β(RH).

[26] The second source is cloud base-height variability. We consider the possibility that lidar β may be biased by the differences in the microphysics between updrafts and downdrafts and how this is observed by lidar. To explore this, a simulation of an adiabatic air parcel is performed. The parcel is raised from a starting RH = 85%, with particles assumed to be NaCl, initially at their equilibrium sizes. Kinetic limitations to growth are simulated. After saturation is reached, the parcel rises further until the cloud-water mixing ratio is about 0.5 g kg^{-1}. It then reverses direction and descends to cloud base and back to the starting RH of 85%. Figure 10 shows this sequence, as well as the simulated backscatter β. In reality, the lidar returned power will attenuate rapidly after the beam has penetrated 2–3 optical depths into the cloud. One can see that in the saturated updraft, cloud base (RH = 100%) is at 478 m. The downdraft is not quite saturated because of the inertia of drops to evaporation, and cloud base is less clearly defined. If one assumes that it is located at the same point on the β profile, which would be the case if the same detection algorithm were used, then cloud base is at 460 m, i.e., 18 m lower. However, the calculations assume that this point is saturated, whereas in reality the saturation altitude would be somewhat higher. Correction for this effect would amount to assuming a higher cloud base (as in Figure 7) which amounts to a larger f_β(RH).

[27] Figure 9 is suggestive, but quite different from, the "hysteresis effect" that is a well-known feature of pure organic salts [*Tang and Munkelwitz*, 1994]. A pure salt that is exposed to increasing levels of RH will not grow until its deliquescence point is reached. For NaCl this is at ~75% RH. At this point, growth is rapid with increasing RH. When RH decreases, the particles follow their growth curves back down to the deliquescence point. With further decrease in RH they depart their growth curves; they are larger at a given RH because the hydrated particle must work to evaporate water and crystallize a salt particle in order to achieve the lower-energy state of a solid particle.

5.4. Relationship Between Lidar and Nephelometer-Derived Growth Factors

[28] Since the nephelometer-derived f(RH) is the current standard for quantifying aerosol uptake of water vapor, we perform some calculations of both parameters for prescribed aerosol size distributions. From Figure 4 we assume a mean lognormal size distribution with equivalent mean $N_a = 174$ cm^{-3}, $\bar{r} = 0.08$ μm, and $D = 0.52$ for the period 13.0–13.5 UTC. We then calculate the equivalent f_β(RH) (backscatter) and f(RH) (nephelometer) at a range of RH for

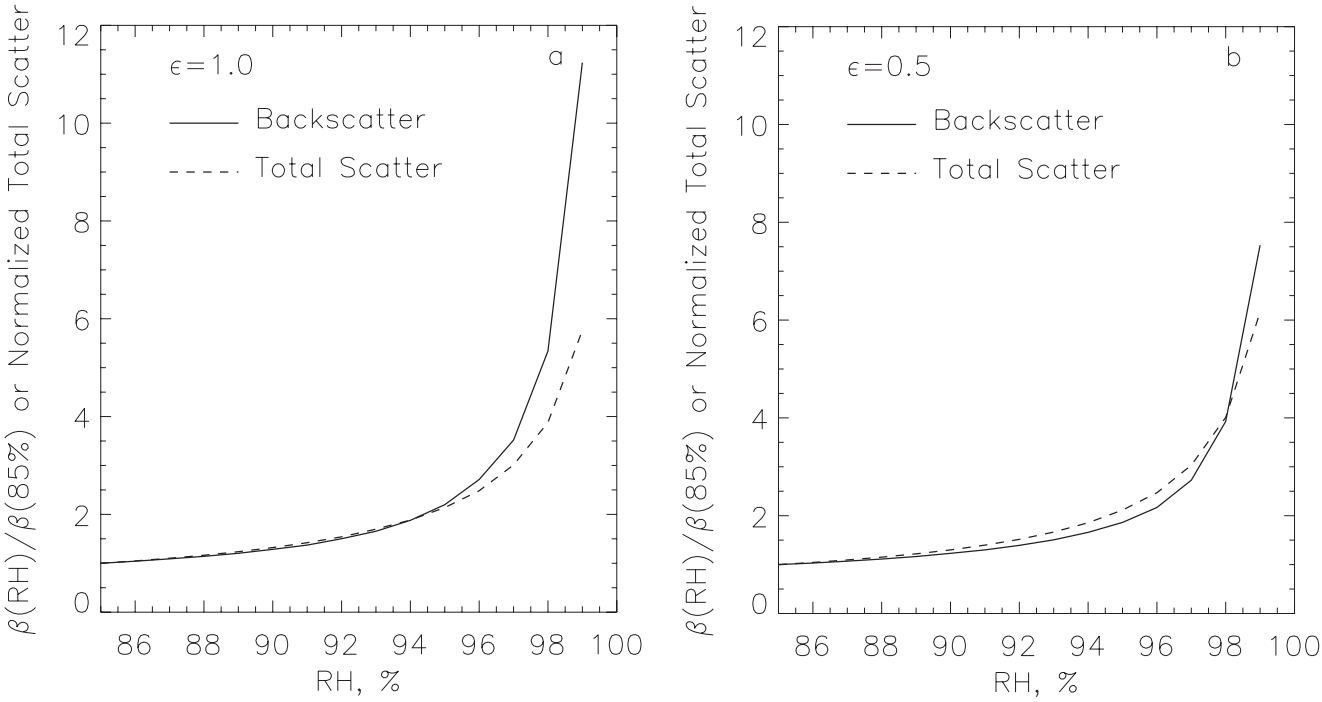

Figure 11. Comparison of aerosol backscatter and total scatter calculations for the mean size distribution: (a) mass fraction of NaCl (ϵ) = 1.0 and (b) ϵ = 0.5.

(1) fully soluble NaCl particles (ϵ = 1) or (2) partially soluble NaCl particles (ϵ = 0.5). Figure 11a shows that for fully soluble NaCl particles the normalized f_β(RH) is larger than the normalized f(RH) for RH > 95% with the difference increasing as saturation is approached. When the particles are only partially soluble, the differences are less marked, and f(RH) > f_β(RH) for 90% < RH < 98%. Conversely, f_β(RH) > f(RH) for RH > 98%. In general, however, for RH < 95% the similarity between f_β(RH) and f(RH) is such that f_β(RH) may be directly applicable. To explore this further, Figure 12 performs similar calculations at values of RH (92% and 98%) and two values of ϵ (0.5 and 1.0) and for a range of lognormal size distribution parameters r_g (median size) and σ (geometric standard deviation). The equivalent mean radius $\bar{r}$ and relative dispersion D can be calculated using $\bar{r} = r_g \exp(0.5\ ln^2\ \sigma)$, and $D = (\exp(ln^2\ \sigma) - 1)^{1/2}$. Figure 12 shows contours of the ratio of f_β(RH) to f(RH). It can be seen that at RH = 92%, f_β(RH) is within 10–20% of f(RH) for a wide range of size distribution parameter space, regardless of ϵ. When RH = 98%, the differences are much larger, and f_β(RH) can be a factor of 0.5 × f(RH) to a factor of 2 × f(RH) (depending on the size distribution), with some dependence on ϵ.

6. Summary

[29] We have shown how a single-wavelength backscatter lidar (0.532 μm) can be used to derive information on the growth properties of aerosol particles when the boundary layer is well mixed and capped by clouds. The fundamental premise is that under these conditions, increases in lidar backscatter with increasing RH can be assumed to be associated with aerosol uptake of water vapor. This work therefore extends that of *Wulfmeyer and Feingold* [2000], who used a differential absorption lidar to derive information on the uptake of water vapor by aerosols. In the current study, the in situ measurement of potential temperature and pressure is used to calculate a temperature profile. Using cloud base as a calibration point of 100% RH, the cloud base water vapor mixing ratio is derived. Then, assuming that water vapor is also well mixed, the RH profile is calculated. The results are presented as a normalized growth factor which is termed f_β(RH).

[30] In situ aerosol size and composition measurements are used to calculate the expected backscatter as a function of RH, and results compare favorably with the lidar results. This comparison was facilitated by the fact that the aerosol particles were predominantly sodium chloride. The differences between the two calculations are well within the errors associated with the derivation of f_β(RH) inherent in the lidar method, as well as those associated with sizing of particles with the optical device (PCASP). In addition, the 1-s sample-to-sample variabilty in f_β(RH) tends to be larger than the variability in the mean f_β(RH) because of assumptions made in deriving each individual f_β(RH).

[31] Conditional sampling shows that downdrafts tend to have stronger f_β(RH) than updrafts do at the same RH. It is suggested that this is a result of the time constant associated with growth/evaporation and the particles' inertia to size change. In stronger up/downdrafts, particles do not have sufficient time to reach their equilibrium sizes; growing particles tend to lag behind in size, whereas evaporating particles tend to be larger. It may also be due to a bias in the way that lidar-derived cloud base is interpreted in updrafts versus downdrafts, which then biases the derived RH profiles.

[32] It is shown that the lidar backscatter f_β(RH) may differ significantly from that of the commonly used f(RH) based on

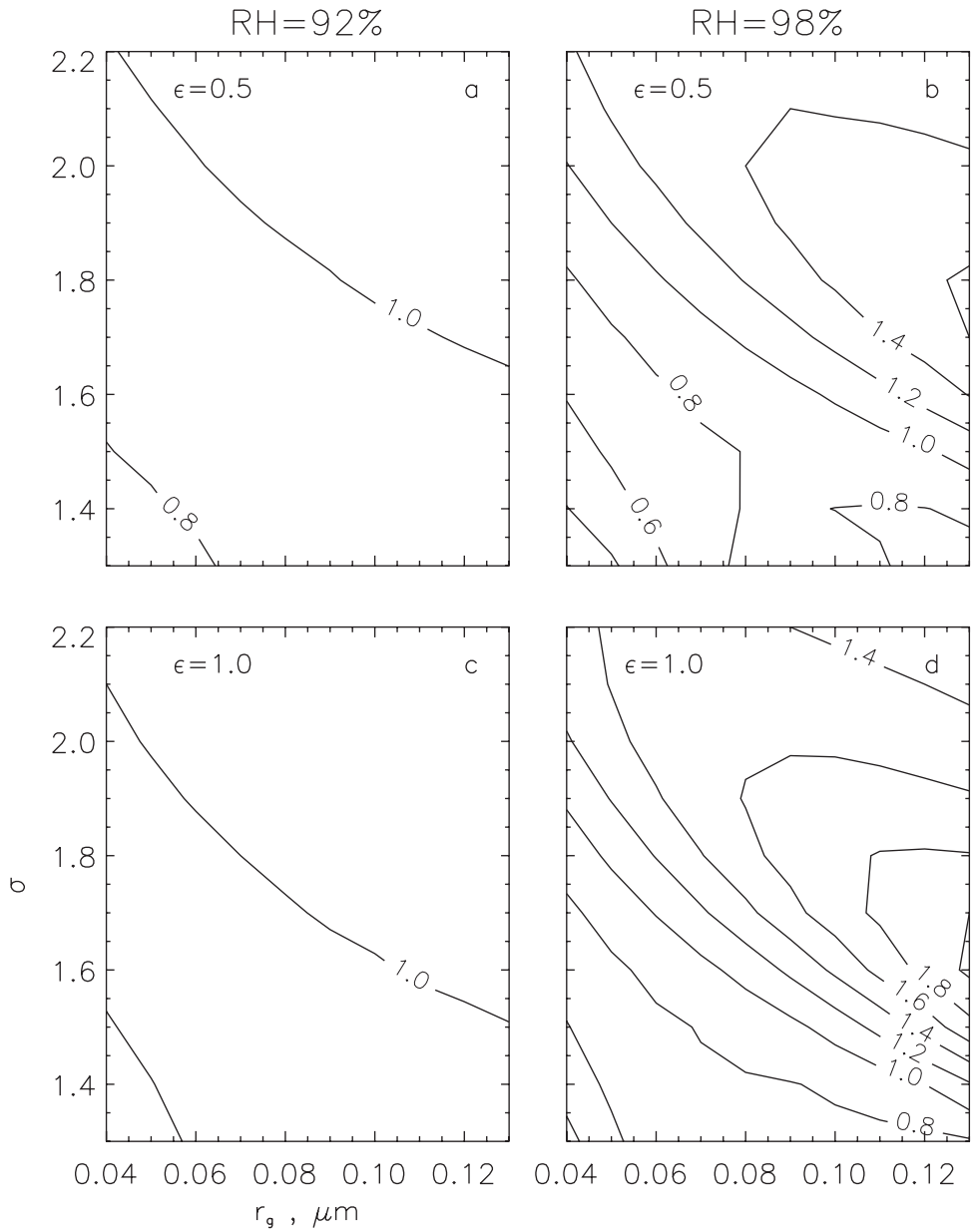

Figure 12. Contours of the ratio of f_β(RH) to f(RH) for a range of lognormal size distribution parameters: r_g (median radius) and σ (geometric standard deviation). (a) RH = 92% and ϵ = 0.5, (b) RH = 98% and ϵ = 0.5, (c) RH = 92% and ϵ = 1.0, (d) RH = 98% and ϵ = 1.0. The contour interval is 0.2.

humidified nephelometers, particularly at RH > ~95%, where f_β(RH) > f(RH). The extent of this disagreement is dependent on the size distribution and composition of the aerosol. However, over the range 85% < RH < 95%, f_β(RH) and f(RH) are in reasonable agreement for the conditions explored here. The main advantage of the lidar method over that of the nephelometer-based method is that (1) lidar can extend the range of measurement to close to saturation and (2) lidar measures the aerosol uptake of water vapor in ambient, unperturbed conditions. Although aerosol backscatter is not necessarily the parameter of choice for measuring the radiative effects of aerosol particles, the possibility it offers for long-term monitoring of aerosol growth parameters, as well as the fundamental advantages of the lidar approach, are appealing. It is therefore suggested that broad application of backscatter lidars in well-mixed, cloud-capped boundary layers could provide a source of valuable information for addressing the aerosol direct and indirect effects.

[33] **Acknowledgments.** The authors are grateful to the entire team of scientists and support staff who made the DYCOMS-II field experiment possible. Useful discussions with Volker Wulfmeyer, Patrick Y. Chuang, Christoph Senff, Wynn L. Eberhard, Jefferson R. Snider, Jenny Hand, and Dan Murphy are much appreciated. Two anonymous reviewers are thanked for their useful comments.

References

Anderson, T. L., S. J. Masonis, D. S. Covert, R. J. Charlson, and M. J. Rood, In situ measurement of the aerosol extinction to backscatter ratio at a polluted continental site, *J. Geophys. Res.*, *105*, 26,907–26,915, 2000.

Brechtel, F. J., and S. M. Kreidenweis, Predicting particle critical supersaturation from hygroscopic growth measurements in the humidified

TDMA. part II: Laboratory and ambient studies, *J. Atmos. Sci.*, *57*, 1872–1887, 2000.

Brenguier, J. L., et al., An overview of the ACE-2 CLOUDYCOLUMN closure experiment, *Tellus, Ser. B*, *52*, 815–827, 2000.

Charlson, R. J., D. S. Covert, and T. V. Larson, Observations of the effect of humidity on light scattering by aerosols, in *Hygroscopic Aerosols*, edited by T. H. Ruhnke and A. Deepak, pp. 35–44, A. Deepak, Hampton, Va., 1984.

Charlson, R. J., S. E. Schwartz, J. M. Hales, R. D. Cess, J. A. Coakley Jr., J. E. Hansen, and D. J. Hofmann, Climate forcing by anthropogenic aerosols, *Science*, *255*, 423–430, 1992.

de Leeuw, G., G. J. Kunz, and C. W. Lamberts, Humidity effects on the backscatter/extinction ratio, *Appl. Opt.*, *25*, 3971–3974, 1986.

Eichel, C., M. Krämer, L. Schütz, and S. Wurzler, The water soluble fraction of atmospheric aerosol particles and its influence on cloud microphysics, *J. Geophys. Res.*, *101*, 29,499–29,510, 1996.

Feingold, G., B. Stevens, W. R. Cotton, and R. L. Walko, An explicit microphysics/LES model designed to simulate the Twomey Effect, *Atmos. Res.*, *33*, 207–233, 1994.

Ferrare, R. A., S. H. Melfi, D. N. Whiteman, K. D. Evans, M. Poellot, and Y. J. Kaufman, Raman lidar measurements of aerosol extinction and backscattering: 2. Derivation of aerosol real refractive index, single-scattering albedo, and humidification factor using Raman lidar and aircraft size distribution measurements, *J. Geophys. Res.*, *103*, 19,673–19,690, 1998.

Hand, J., R. B. Ames, S. M. Kreidenweis, D. E. Day, and W. C. Malm, Estimates of particle hygroscopicity during the southeastern aerosol and visibility study, *J. Air Waste Manage. Assoc.*, *50*, 677–685, 2000.

Hansen, J. E., M. Sato, and R. Ruedy, Radiative forcing and climate response, *J. Geophys. Res.*, *102*, 6831–6864, 1997.

Hegg, D. A., D. S. Covert, M. J. Rood, and P. V. Hobbs, Measurements of aerosol optical properties in marine air, *J. Geophys. Res.*, *101*, 12,893–12,903, 1996.

Jiang, H., G. Feingold, and W. R. Cotton, A modeling study of entrainment of cloud condensation nuclei into the marine boundary layer during ASTEX, *J. Geophys. Res.*, *107*(D24), 4813, doi:10.1029/2001JD001502, 2002.

McInnes, L., M. Bergin, and J. Ogren, Apportionment of light scattering and hygroscopic growth to aerosol composition, *Geophys. Res. Lett.*, *25*, 513–516, 1998.

Pruppacher, H. R., and J. D. Klett, *Microphysics of Clouds and Precipitation*, 954 pp., Kluwer Acad., Norwell, Mass., 1997.

Stevens, B., et al., Dynamics and chemistry of marine stratocumulus—DYCOMS-II, *Bull. Am. Meteorol. Soc.*, *84*, 579–593, 2003.

Tang, I. N., and H. R. Munkelwitz, Water activities, densities, and refractive indices of aqueous sulfates and sodium nitrate droplets of atmospheric importance, *J. Geophys. Res.*, *99*, 18,801–18,808, 1994.

Twomey, S., Pollution and the planetary albedo, *Atmos. Environ.*, *8*, 1251–1256, 1974.

Wulfmeyer, V., and G. Feingold, On the relationship between relative humidity and particle backscattering coefficient in the marine boundary layer determined with differential absorption lidar, *J. Geophys. Res.*, *105*, 4729–4741, 2000.

G. Feingold, NOAA Environmental Technology Laboratory, 325 Broadway, Boulder, CO 80305, USA. (graham.feingold@noaa.gov)

B. Morley, Atmospheric Technology Division, National Center for Atmospheric Research, Boulder, CO 80307, USA. (bruce@atd.ucar.edu)